The Holocene OnlineFirst, published on August 12, 2010 as doi:10.1177/0959683610374883

Research paper

The Holocene
1–10
© The Author(s) 2010
Reprints and permission:
sagepub.co.uk/journalsPermissions.nav
DOI: 10.1177/0959683610374883
http://hol.sagepub.com
SAGE

Luminescence dating of Holocene sedimentary deposits on Rømø, a barrier island in the Wadden Sea, Denmark

A.T. Madsen,[1] A.S. Murray,[2] T.J. Andersen[1] and M. Pejrup[1]

Abstract

This study presents an Optically Stimulated Luminescence (OSL) based chronology for the evolution of the barrier island Rømø and related back-barrier lagoon deposits in the Danish Wadden Sea. The chronology is constructed using 78 quartz OSL ages obtained using a Single Aliquot Regenerative dose (SAR) protocol; samples were retrieved from seven sediment cores, each up to 25 m long, taken from locations on the island and within the back-barrier lagoon. The reliability of the OSL results is assessed using preheat plateaus, thermal transfer tests, and dose recovery measurements, and by comparison with independent age control. The OSL ages compare favourably with three ^{14}C age estimates, and range between 220±20 and 15 800±1200 years. Rømø appears to have developed as a progradational barrier system, and the island appeared for the first time approximately 8000 years ago. It then gradually expanded towards the west, north and south as a result of an abundant sediment supply. Luminescence dating is concluded to be well-suited for establishing precise and accurate chronologies for barrier island deposits, and the technique has provided an excellent basis for the reconstruction of barrier island evolution.

Keywords

barrier island, OSL, quartz, SAR protocol, sea level, ^{14}C

Introduction

This paper investigates the absolute dating of Holocene sedimentary deposits, resulting from the evolution of a barrier island system. Since the last glacial maximum (LGM) about 20 000 years ago, global sea level has been rising significantly through the melting of glacial ice on a global scale (eustasy), but with local modulations arising from crustal response to deglaciation (isostasy). The isostatic land movements resulting from the unloading after the ice retreat have varied considerably on a global scale, resulting in a large spatial variation in relative sea-level changes (Bird, 1993) but the overall trend has been a rise in global mean sea level during the Holocene. Given the probable effects of future climate change sea-level rise is likely to have a large effect on coastal areas made up of soft sediments, such as barrier coasts (Intergovernmental Panel on Climate Change (IPCC), 2007). These effects may include re-shaping of coastal morphology and physical and social impacts on human populations living on barrier islands and in coastal regions. The understanding of the response of coastal barrier systems to sea-level rise is thus important from both scientific and management perspectives.

The response of barrier island systems to relative sea-level rise has been the subject of a number of previous studies (Dean and Maurmeyer, 1983; Flemming, 2002; Komar *et al*., 1991; Leatherman, 1983; Nummedal, 1983; Thom, 1983) and overviews of barrier island systems have been given by Oertel (1985) and Davis (1994). These authors conclude that a long-term rise in sea level generally results in a landward migration of barrier islands (i.e. such barrier systems are transgressive). However, the barrier island response is not always so simple. Some barrier islands have also accreted vertically over the past few thousand years, keeping pace with any increase in sea level (i.e. aggradational barrier systems). In other cases, because of abundant sediment supply, barrier islands have also been prograding despite sea-level rise (i.e. progradational barrier systems). Further investigations are therefore needed to understand the relative importance of changes in sea level and sediment availability on barrier island evolution, and to predict the response of barrier islands to future sea-level rise. Absolute dating of sedimentary deposits is essential to an understanding of when and how the lateral position of a barrier island shifted seawards and/or landwards, and to enable us to relate this to changes in the balance between sea level and availability of sediment throughout the Holocene. In the past, such investigations have often been hampered by the lack of organic material suitable for ^{14}C dating; organic-rich horizons are seldom found in barrier island deposits and shells may have experienced reworking and may therefore result in biased ^{14}C age estimates. Some recent studies, however, have started to apply Optically Stimulated Luminescence (OSL) dating to investigations of barrier island evolution (e.g. Armitage *et al*., 2006; Ballarini *et al*., 2003; Lopez and Rink, 2008; Madsen

[1]University of Copenhagen, Denmark
[2]Aarhus University, Denmark

Received 1 December 2009; revised manuscript accepted 23 April 2010

Corresponding author:
A.T. Madsen, Department of Geography and Geology, University of Copenhagen, Øster Voldgade 10, DK-1350 Copenhagen K, Denmark
Email: atm@geo.ku.dk

et al., 2007). Our paper represents part of a larger study investigating the Holocene evolution of the Danish Wadden Sea; it aims to assess and illustrate the applicability and usefulness of the OSL technique to the dating of the sandy barrier island deposits and back-barrier lagoon deposits in this area.

The main objective of our study is to establish an absolute chronology for the barrier island deposits and to examine the validity of this chronology using both internal tests of reliability and comparisons with external age control. Attention is given to specific laboratory tests undertaken prior to routine OSL measurements; these are intended to validate the technique and to confirm the reliability of the chosen measurement protocol. This study presents 78 OSL dates of the sedimentary deposits of a barrier island and is, to our knowledge, one of the first studies to present such a comprehensive data set. The validity of the OSL ages is discussed by comparison with the more limited independent age estimates available from ^{14}C dating. Finally, the OSL chronology is used to provide a preliminary geological interpretation, which forms the basis for reconstruction of past barrier island evolution.

Study area

The Danish west coast (facing the North Sea) shows evidence of glacial rebound, with land emergence in the north and submergence in the south, as a result of its location at the margin of the late Weichselian Scandinavian Ice Sheet. The barrier island, Rømø, lies just off the submerging Wadden Sea coastline in the southwestern part of Denmark. This area experiences isostatic subsidence due to a forebulge collapse, resulting from the disappearance of ice-pressure behind the bulge. Details on local isostasy and eustasy are given in Gehrels *et al*. (2006) who examined the late-Holocene relative sea-level history and crustal movements in this area. Overall, the area has experienced a relative sea-level rise of about 17 m during the last *c*. 8000 years. However, several sea-level oscillations have taken place (Behre, 2007; Pedersen *et al*., 2009). The last known drop in relative sea level occurred during the 'Little Ice Age' (200–500 years ago; Christiansen *et al*., 1990). Rømø is *c*. 14 km long and up to *c*. 4 km wide (Johannessen *et al*., 2008). The west coast of Rømø, facing the North Sea, has one of the widest beaches in the world (1−1.5 km) because the island lies at the junction of two converging littoral drifts that deliver considerable volumes of sand to the shallow marine sand-flats on the western side of the island. This positive sediment budget results in progradation of the coastline, despite the locally rising relative sea level (Bartholdy and Pejrup, 1994). The island has no glacial sediment core (Moritz, 1903). It is built exclusively of marine and aeolian sand, with some gravel; at least one marine cobble deposit has been identified. Aeolian dune fields cover large parts of Rømø and a shore-parallel ridge and swale system has formed as a result of aeolian sand transport and barrier island progradation. Four well-defined aeolian sand ridges, separated by low-lying swampy areas or swales, border the west coast. Previous investigation of these dune ridges gave average OSL ages of 17±2 years, 22±3 years, 70±6 years and 235±10 years, with the ages increasing inland (Madsen *et al*., 2007). The east coast of Rømø, facing the back-barrier lagoon, is mainly fringed by salt-marsh deposits, with steep *c*. 1 m high erosional margins. A lagoon with tidal flats, protected from the prevailing westerly winds, lies between Rømø and the mainland; these flats have presumably accreted to follow the post-glacial sea-level rise.

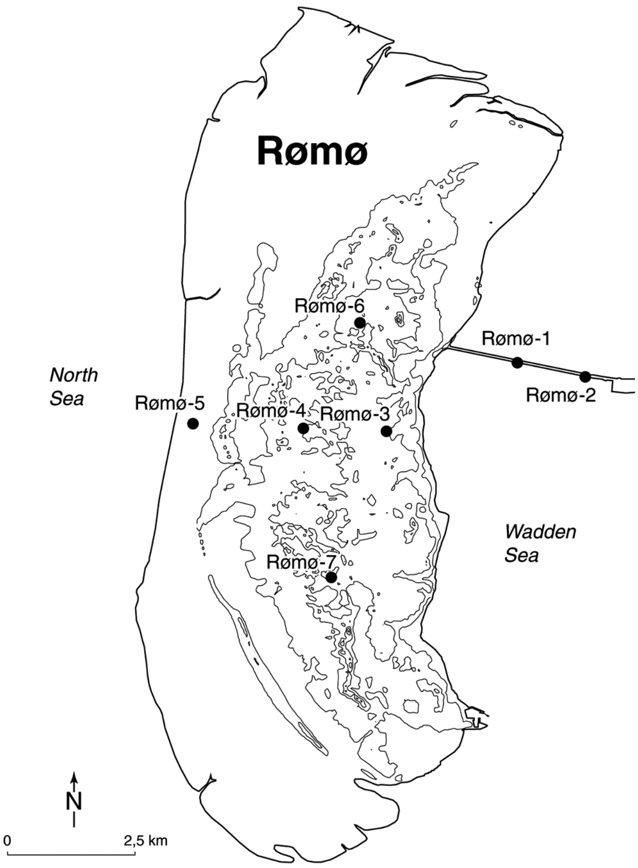

Figure 1. Map displaying the seven sample locations on the barrier island Rømø and the associated tidal lagoon. The contour interval used is 2.5 m. The seven sediment cores were drilled to about 20 m or more below the present surface

Table 1. GPS positions of drilling sites (UTM zone 32N). Elevation is given according to the Danish Vertical Reference from 1990 (DVR90), which datum corresponds to mean sea level

	Northing	Easting	Height (m)
Rømø-1	6,111,507.528	473,446.976	1.911
Rømø-2	6,111,231.014	474,805.272	2.117
Rømø-3	6,110,128.471	470,803.829	4.617
Rømø-4	6,110,180.898	469,101.042	3.952
Rømø-5	6,110,278.215	466,879.816	2.174
Rømø-6	6,112,324.531	470,259.183	4.981
Rømø-7	6,107,156.617	469,672.449	4.583

Methods

Sample recovery

Seven cores were drilled on Rømø and in the adjacent tidal lagoon (Figure 1), using a powered hollow auger lined with 1 m long opaque plastic tubes. Typically, boreholes reached a depth of about 25 m and penetrated well beyond the Holocene material of interest in this study. There was occasionally some loss of the cores at the ends of the 1 m sections, because the material was usually unconsolidated; where possible this loss was allowed for in the reconstruction of the coring depth, but some contamination at the top of each section cannot be ruled out because it was not always possible to detect this by visual examination. The drilling sites (Table 1) were chosen based on Ground Penetrating Radar (GPR) surveys (Nielsen *et al*., 2009).

OSL dating

In the laboratory, the cores were split lengthwise in subdued red light and subsampled with intervals of about 1 m for OSL dating; the samples had vertical ranges of *c*. 25 cm in the core. Each sample (*c*. 500 g) was separated into two portions; one part was used to determine the dose rate using gamma spectrometry and the other part was used for equivalent dose (D_e) measurements. The sample preparation for dose rate determination involved drying to laboratory humidity to determine field water content, ignition at 450°C for 24 h, and subsequent homogenization by grinding to a grain size of about 200 μm or less. The homogenised samples were then mixed with wax, cast in a fixed cup-shaped geometry, and stored for three weeks to allow the establishment of secular equilibrium between ^{222}Rn and ^{226}Ra before counting on a high-resolution gamma ray spectrometer (Murray *et al*., 1987). Saturated water content was measured on a subsample of the unground material; all samples except for 065551 were taken below the present-day water-table, which is known to lie within 1 m of the interdune surfaces on the island. Even sample 065551 had an observed field water content indistinguishable from those lying below the water-table deeper in the core. Because of this, all samples were assumed to be saturated throughout the period of burial and these saturated water contents were used for dose rate calculations.

Quartz grains were extracted from the sediments for D_e measurements. The samples were first sieved to obtain the grain-size fraction 180−250 μm. This fraction was treated with HCl (10%) to dissolve carbonates and other acid-reactive matter. H_2O_2 (10%) was then added to oxidise and remove organic matter, and HF (40%) was added to dissolve feldspar and etch the outer surface of the quartz grains. Finally, the samples were treated with HCl (10%) again to remove any fluorides created during the HF treatment (Aitken, 1985).

The resulting sand-sized quartz grains were mounted on 9.7 mm diameter stainless steel discs, using silicone oil to give a single layer of grains ~8 mm in diameter. Luminescence measurements were undertaken using automated Risø TL/OSL readers equipped with $^{90}Sr/^{90}Y$ beta-sources (Bøtter-Jensen, 1997). The measurements were carried out on five different instruments, having beta sources with strengths varying between 0.09 Gy/s and 0.29 Gy/s. Each reader had a stimulating light source of blue (470±30 nm) light emitting diodes (LEDs) and was fitted with a photomultiplier tube to record the photon counts emitted during the 40 s of optical stimulation; U-340 transmission filters were used to reject the stimulating light. The OSL signal used was the integral of the initial 0.8 s of the decay curve, less a background derived from the interval 4.8 to 5.6 s in the decay curve (see Figure 2 inset).

A Single Aliquot Regenerative dose (SAR) protocol was used to determine D_e (Murray and Wintle, 2000, 2003). For older samples, a 10 s preheat at 260°C prior to regeneration dose measurements and heating to 220°C prior to test dose measurements was used. For samples with D_e values <5 Gy, a 10 s preheat at 200°C prior to regeneration dose measurements and heating to 180°C prior to test dose measurements was used to minimise the risk of thermal transfer (see later). In the SAR protocol the sensitivity-corrected natural OSL signal is first measured, then the responses to three, or more, laboratory doses are measured to build up a growth curve upon which the natural response can be interpolated (solid circles Figure 2). Potential sensitivity changes that may occur during the measurement procedure are corrected by measuring the response to a constant test dose after each laboratory dose and then dividing each

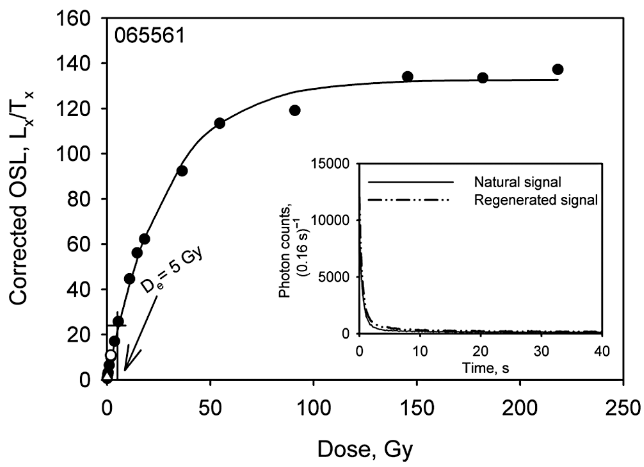

Figure 2. Typical example of an OSL growth curve where solid circles represent OSL responses to different laboratory doses, and the open circle is a recycling point. The open triangle is the recuperation signal. The inset displays the natural OSL signal together with the OSL signal from a regenerative laboratory dose of approximately the same size

dose response with the following test dose response. The test doses applied in this study varied between 0.8 and 16 Gy, depending on the size of the natural dose being measured. The measurement of the luminescence response to each laboratory dose and corresponding test doses is followed by a measurement of the response to zero dose (open triangle Figure 2) to observe any significant thermally transferred recuperation of the luminescence signal resulting from heating. Finally, one of the laboratory doses is repeated (the recycling test) to check that it is possible to measure a similar response from a repeated dose (open circle, Figure 2). The latter two tests, measuring the recuperation and the recycling ratio, allow routine checks on the reliability of results from individual aliquots of a sample; typically D_e (Tables 2−8) measurements are based on results from 12−33 aliquots per sample.

Radiocarbon dating

Organic material, small wood fragments, suitable for ^{14}C dating was found in two of the cores (Rømø-1 and Rømø-6). These samples were radiocarbon dated at the University of Kiel to provide independent age control, and the radiocarbon ages are presented as calibrated radiocarbon years before present (AD 1950) using CALIB rev. 5.01 (Reimer *et al*., 2004).

Results

Luminescence characteristics

A number of laboratory tests were undertaken on quartz extracted from the cores prior to routine application of the SAR protocol. The tests were designed in order to measure the variation in the apparent equivalent dose with preheat temperature (Murray and Wintle, 2000), to quantify the extent of thermal transfer, if any (Rhodes, 2000), and to check if it is possible to recover a known laboratory dose (Wallinga *et al*., 2000).

Twenty-four aliquots of sample 065561 were used to illustrate the variation in the apparent equivalent dose (D_e) as a function of preheat temperature, using eight different preheat temperatures from 160 to 300°C; three aliquots were measured at each preheat

Table 2. Sample depth, water content, equivalent doses, dose rates and OSL ages from the Rømø-1 core

Sample code	Depth (cm)	w.c. (%)	n	D_e (Gy)	^{238}U (Bq/kg)	^{226}Ra (Bq/kg)	^{232}Th (Bq/kg)	^{40}K (Bq/kg)	Dose rate (Gy/ka)	OSL age (yr)
075506	490	38	33	0.9 ± 0.03	10.1 ± 2.5	9.6 ± 0.2	9.7 ± 0.2	287 ± 5	1.03 ± 0.04	850 ± 50
075507	565	34	21	0.8 ± 0.1	12.5 ± 5.2	8.3 ± 0.4	9.4 ± 0.9	476 ± 10	1.45 ± 0.06	550 ± 50
075508	640	31	21	2.9 ± 0.1	9.8 ± 3.0	7.2 ± 0.2	6.1 ± 0.2	304 ± 6	1.02 ± 0.05	2800 ± 160
075509	790	36	21	7.5 ± 0.2	20.3 ± 4.3	13.8 ± 0.4	12.2 ± 0.4	383 ± 7	1.31 ± 0.05	5700 ± 300
075510	858	36	21	8.1 ± 0.1	16.7 ± 4.4	15.1 ± 0.4	15.6 ± 0.4	447 ± 10	1.49 ± 0.06	5500 ± 300
075511	921	30	20	6.0 ± 0.2	17.9 ± 7.1	12.1 ± 0.5	10.3 ± 0.6	357 ± 9	1.25 ± 0.06	4800 ± 300
075512	1225	30	21	7.4 ± 0.2	15.0 ± 4.9	11.6 ± 0.4	10.6 ± 0.4	351 ± 8	1.21 ± 0.05	6100 ± 300
075513	1372	38	21	8.2 ± 0.2	2.8 ± 4.0	9.6 ± 0.3	8.0 ± 0.3	295 ± 7	1.14 ± 0.05	7100 ± 400
075514	1499	34	21	12.6 ± 0.5	11.9 ± 6.1	7.1 ± 0.5	7.9 ± 0.5	284 ± 8	0.94 ± 0.05	13 500 ± 900
075515	1527	25	19	11.1 ± 0.3	6.0 ± 4.0	5.8 ± 0.3	4.9 ± 0.3	270 ± 7	0.89 ± 0.05	12 500 ± 800

Table 3. Sample depth, water content, equivalent doses, dose rates and OSL ages from the Rømø-2 core

Sample code	Depth (cm)	w.c. (%)	n	D_e (Gy)	^{238}U (Bq/kg)	^{226}Ra (Bq/kg)	^{232}Th (Bq/kg)	^{40}K (Bq/kg)	Dose rate (Gy/ka)	OSL age (yr)
065538	270	42	18	2.4 ± 0.3	29.4 ± 6.8	17.3 ± 0.5	21.2 ± 0.6	412 ± 9	1.55 ± 0.06	1580 ± 230
065539	370	35	17	3.0 ± 0.1	30.2 ± 5.7	16.9 ± 0.5	19.5 ± 0.5	438 ± 9	1.64 ± 0.06	1800 ± 90
065540	460	32	19	3.8 ± 0.3	19.0 ± 13.6	17.6 ± 1.0	18.9 ± 1.1	448 ± 16	1.64 ± 0.08	2300 ± 200
065541	515	27	21	3.0 ± 0.1	20.3 ± 8.7	13.5 ± 0.6	14.6 ± 0.7	397 ± 12	1.49 ± 0.07	1990 ± 130
075518	707	24	18	4.8 ± 0.1	14.6 ± 5.4	13.4 ± 0.4	12.7 ± 0.5	370 ± 9	1.40 ± 0.06	3500 ± 200
065542	715	38	21	6.4 ± 0.1	26.4 ± 9.1	20.0 ± 0.8	22.1 ± 0.8	432 ± 13	1.60 ± 0.07	4000 ± 200
065543	843	32	18	7.1 ± 0.2	25.1 ± 11.2	14.3 ± 0.8	12.4 ± 0.9	381 ± 13	1.36 ± 0.37	5200 ± 1400
065544	915	27	18	19.1 ± 0.9	15.3 ± 8.6	12.8 ± 0.6	9.6 ± 0.7	329 ± 11	1.21 ± 0.06	15 800 ± 1200

Table 4. Sample depth, water content, equivalent doses, dose rates and OSL ages from the Rømø-3 core

Sample code	Depth (cm)	w.c. (%)	n	D_e (Gy)	^{238}U (Bq/kg)	^{226}Ra (Bq/kg)	^{232}Th (Bq/kg)	^{40}K (Bq/kg)	Dose rate (Gy/ka)	OSL age (yr)
075519	272	26	18	1.26 ± 0.04	–0.6 ± 4.4	2.8 ± 0.3	2.7 ± 0.4	138 ± 6	0.60 ± 0.04	2110 ± 160
075520	447	23	18	1.26 ± 0.04	9.5 ± 4.5	3.8 ± 0.3	4.2 ± 0.3	133 ± 4	0.63 ± 0.04	1990 ± 140
075521	572	28	18	1.28 ± 0.04	2.5 ± 4.3	5.6 ± 0.3	5.5 ± 0.4	150 ± 6	0.65 ± 0.04	1970 ± 140
075522	830	48	18	4.42 ± 0.08	29.3 ± 9.4	8.1 ± 0.7	6.7 ± 0.7	287 ± 11	0.93 ± 0.05	4800 ± 300
075523	960	40	18	5.7 ± 0.1	15.2 ± 6.1	10.8 ± 0.4	8.1 ± 0.5	277 ± 8	0.94 ± 0.05	6000 ± 300
075524	1045	35	17	5.5 ± 0.2	9.9 ± 5.0	5.1 ± 0.4	4.2 ± 0.4	223 ± 8	0.74 ± 0.04	7400 ± 500
075525	1145	32	18	6.6 ± 0.3	10.3 ± 7.5	4.8 ± 0.5	4.6 ± 0.6	226 ± 9	0.76 ± 0.05	8600 ± 700
075526	1237	39	24	7.0 ± 0.4	2.7 ± 5.6	4.7 ± 0.4	3.4 ± 0.4	176 ± 7	0.58 ± 0.04	12 100 ± 1100
075527	1342	40	17	4.5 ± 0.2	7.5 ± 5.7	4.2 ± 0.4	4.7 ± 0.5	202 ± 8	0.65 ± 0.04	6900 ± 500
075528	1422	41	20	4.9 ± 0.2	11.8 ± 7.2	4.3 ± 0.5	3.7 ± 0.6	185 ± 8	0.61 ± 0.04	8000 ± 600

Table 5. Sample depth, water content, equivalent doses, dose rates and OSL ages from the Rømø-4 core

Sample code	Depth (cm)	w.c. (%)	n	D_e (Gy)	^{238}U (Bq/kg)	^{226}Ra (Bq/kg)	^{232}Th (Bq/kg)	^{40}K (Bq/kg)	Dose rate (Gy/ka)	OSL age (yr)
065551	48	23	16	0.42 ± 0.04	6.3 ± 6.7	3.2 ± 0.5	3.7 ± 0.6	223 ± 10	0.92 ± 0.05	450 ± 50
065552	143	27	16	0.75 ± 0.02	14.4 ± 8.1	5.6 ± 0.6	6.7 ± 0.6	209 ± 8	0.91 ± 0.05	820 ± 50
065553	260	20	16	0.81 ± 0.02	–1.7 ± 4.2	3.7 ± 0.3	3.2 ± 0.3	210 ± 5	0.82 ± 0.04	990 ± 60
065554	338	30	16	0.95 ± 0.03	9.5 ± 4.5	4.7 ± 0.3	5.5 ± 0.4	269 ± 7	0.96 ± 0.05	980 ± 60
065555	440	21	18	0.83 ± 0.03	17.4 ± 10.7	4.1 ± 0.7	4.2 ± 0.8	139 ± 10	0.69 ± 0.05	1200 ± 100
065556	539	28	19	1.49 ± 0.03	7.1 ± 7.4	5.7 ± 0.5	5.9 ± 0.6	298 ± 10	1.03 ± 0.05	1450 ± 80
065557	640	22	17	1.49 ± 0.03	13.0 ± 7.7	4.4 ± 0.6	4.0 ± 0.6	223 ± 10	0.85 ± 0.05	1740 ± 110
065558	742	20	17	2.07 ± 0.09	0.5 ± 9.3	4.2 ± 0.7	4.4 ± 0.7	155 ± 9	0.68 ± 0.05	3000 ± 300
065559	946	31	17	4.31 ± 0.08	3.1 ± 6.2	4.1 ± 0.4	3.9 ± 0.5	252 ± 8	0.81 ± 0.04	5300 ± 300
065560	1028	31	20	4.73 ± 0.06	2.3 ± 6.8	7.0 ± 0.5	5.9 ± 0.6	330 ± 11	1.02 ± 0.05	4600 ± 300
065561	1140	33	18	4.92 ± 0.06	9.7 ± 5.6	9.0 ± 0.5	7.6 ± 0.5	271 ± 11	0.93 ± 0.05	5300 ± 300
065562	1238	25	19	5.41 ± 0.07	34.2 ± 12.3	7.9 ± 0.9	6.9 ± 0.9	260 ± 13	1.02 ± 0.06	5300 ± 400
065563	1327	29	16	5.2 ± 0.1	–0.3 ± 7.4	6.9 ± 0.5	5.1 ± 0.6	264 ± 9	0.85 ± 0.05	6100 ± 400
065564	1444	28	18	7.2 ± 0.1	9.1 ± 7.2	11.9 ± 0.6	10.2 ± 0.6	346 ± 11	1.18 ± 0.06	6100 ± 300

temperature. For this sample, estimates of D_e proved to be essentially independent of temperature in the preheat range of 180–280°C (Figure 3) with a mean value of 4.92±0.06 Gy (n=18), corresponding to an age of *c*. 5300 years. At higher preheat temperatures (300°C) the apparent D_e estimate is significantly higher. This increase in D_e may be related to thermal transfer, but this is tested in the next laboratory test.

Twenty-four new aliquots of sample 065561 were prepared to test for the presence of thermal transfer. These were firstly bleached for 40 s, using blue LEDs (at room temperature), then held for 10 000 s, to allow any charge transferred to the 110°C TL trap (Wintle, 1997) to decay, and finally given a further optical bleach for 40 s. The apparent dose was then measured, using a SAR protocol with eight different preheat temperatures. The thermal dependence of

Table 6. Sample depth, water content, equivalent doses, dose rates and OSL ages from the Rømø-5 core

Sample code	Depth (cm)	w.c. (%)	*n*	D_e (Gy)	^{238}U (Bq/kg)	^{226}Ra (Bq/kg)	^{232}Th (Bq/kg)	^{40}K (Bq/kg)	Dose rate (Gy/ka)	OSL age (yr)
065569	133	26	18	0.29 ± 0.02	9.3 ± 8.4	5.6 ± 0.6	5.9 ± 0.7	318 ± 13	1.15 ± 0.06	250 ± 20
065570	240	27	18	0.25 ± 0.01	7.6 ± 10.5	8.2 ± 0.7	9.1 ± 0.9	294 ± 12	1.13 ± 0.06	220 ± 20
065571	358	30	18	0.30 ± 0.02	9.9 ± 6.4	4.8 ± 0.4	4.4 ± 1.0	334 ± 9	1.09 ± 0.05	230 ± 20
065572	340	30	18	0.31 ± 0.02	20.6 ± 11.3	5.7 ± 0.8	5.9 ± 0.9	362 ± 14	1.22 ± 0.06	250 ± 20
065573	530	18	18	0.23 ± 0.01	4.0 ± 6.8	4.1 ± 0.5	3.9 ± 0.6	122 ± 8	0.60 ± 0.04	390 ± 30
065574	683	32	12	0.36 ± 0.01	2.9 ± 9.4	4.6 ± 0.7	4.6 ± 0.7	282 ± 11	0.89 ± 0.05	400 ± 30
065575	778	28	17	0.36 ± 0.01	−4.0 ± 8.6	6.4 ± 0.6	4.2 ± 0.6	308 ± 11	0.97 ± 0.05	380 ± 30
065576	1043	30	18	3.11 ± 0.06	9.0 ± 7.0	6.1 ± 0.5	5.0 ± 0.6	280 ± 11	0.92 ± 0.05	3380 ± 200
065577	1128	28	18	3.11 ± 0.07	4.1 ± 6.1	4.9 ± 0.5	4.7 ± 0.5	252 ± 9	0.83 ± 0.05	3700 ± 200
065578	1240	32	18	3.02 ± 0.06	7.2 ± 9.0	6.0 ± 0.6	3.5 ± 0.7	258 ± 10	0.81 ± 0.05	3700 ± 200
065579	1340	29	17	4.28 ± 0.21	12.5 ± 10.5	10.1 ± 0.8	10.4 ± 0.8	356 ± 13	1.21 ± 0.06	3500 ± 300
065580	1440	25	18	4.60 ± 0.16	10.6 ± 5.8	6.6 ± 0.5	7.1 ± 0.5	238 ± 10	0.88 ± 0.05	5300 ± 400
065581	1540	27	18	13 ± 1	9.5 ± 8.0	9.6 ± 0.6	4.9 ± 0.6	281 ± 10	0.99 ± 0.05	13 300 ± 1000

Table 7. Sample depth, water content, equivalent doses, dose rates and OSL ages from the Rømø-6 core

Sample code	Depth (cm)	w.c. (%)	*n*	D_e (Gy)	^{238}U (Bq/kg)	^{226}Ra (Bq/kg)	^{232}Th (Bq/kg)	^{40}K (Bq/kg)	Dose rate (Gy/ka)	OSL age (yr)
075535	112	24	18	0.56 ± 0.02	0.6 ± 2.9	3.8 ± 0.2	3.0 ± 0.2	215 ± 5	0.84 ± 0.04	670 ± 40
075536	235	28	18	0.92 ± 0.02	6.1 ± 2.6	3.4 ± 0.2	4.0 ± 0.2	158 ± 4	0.69 ± 0.04	1330 ± 80
075537	325	26	18	1.02 ± 0.03	7.8 ± 7.0	4.8 ± 0.5	4.6 ± 0.5	152 ± 7	0.69 ± 0.04	1470 ± 100
075538	565	22	18	1.33 ± 0.03	1.2 ± 6.2	4.0 ± 0.4	2.7 ± 0.5	177 ± 7	0.68 ± 0.04	1940 ± 140
075539	655	29	18	1.69 ± 0.05	13.9 ± 11.1	4.6 ± 0.8	4.3 ± 0.8	289 ± 12	0.97 ± 0.06	1750 ± 120
075540	775	32	16	2.72 ± 0.09	25.0 ± 7.8	8.6 ± 0.6	8.3 ± 0.7	339 ± 12	1.17 ± 0.06	2320 ± 140
075541	865	23	17	3.54 ± 0.14	1.7 ± 7.3	5.5 ± 0.5	3.5 ± 0.5	246 ± 9	0.85 ± 0.05	4200 ± 300
075542	965	22	18	2.86 ± 0.11	7.5 ± 11.8	4.1 ± 0.8	2.3 ± 0.9	184 ± 11	0.68 ± 0.06	4200 ± 400
075543	1060	23	18	2.64 ± 0.09	5.5 ± 5.5	3.7 ± 0.4	3.2 ± 0.5	157 ± 7	0.61 ± 0.04	4300 ± 300
075544	1245	31	18	4.27 ± 0.09	−0.9 ± 7.2	3.8 ± 0.5	2.5 ± 0.5	291 ± 9	0.84 ± 0.05	5100 ± 300
075545	1570	23	18	4.61 ± 0.10	10.0 ± 8.9	6.2 ± 0.6	5.4 ± 0.7	255 ± 9	0.90 ± 0.05	5100 ± 300
075546	1670	47	18	5.62 ± 0.13	10.0 ± 3.5	3.9 ± 0.3	3.5 ± 0.3	211 ± 6	0.62 ± 0.04	9100 ± 600
075547	1760	35	18	6.64 ± 0.16	5.1 ± 5.8	6.3 ± 0.4	5.0 ± 0.1	319 ± 8	0.93 ± 0.05	7200 ± 400
075548	1830	32	18	8.60 ± 0.15	19.6 ± 5.9	11.9 ± 0.5	10.6 ± 0.5	351 ± 10	1.19 ± 0.05	7200 ± 400
075549	2053	29	17	6.62 ± 0.19	3.1 ± 7.5	6.5 ± 0.5	5.8 ± 0.6	257 ± 9	0.83 ± 0.05	8000 ± 500
075550	2240	28	18	11 ± 0.4	13.4 ± 14.0	9.1 ± 1.0	8.9 ± 1.1	344 ± 15	1.13 ± 0.07	10 000 ± 700

Table 8. Sample depth, water content, equivalent doses, dose rates and OSL ages from the Rømø-7 core

Sample code	Depth (cm)	w.c. (%)	*n*	D_e (Gy)	^{238}U (Bq/kg)	^{226}Ra (Bq/kg)	^{232}Th (Bq/kg)	^{40}K (Bq/kg)	Dose rate (Gy/ka)	OSL age (yr)
075552	247	36	18	0.68 ± 0.02	0.5 ± 8.8	4.8 ± 0.6	2.9 ± 0.7	282 ± 11	0.90 ± 0.05	750 ± 50
075553	330	34	18	0.96 ± 0.03	−2.3 ± 8.2	5.8 ± 0.6	4.4 ± 0.6	251 ± 10	0.86 ± 0.05	1120 ± 70
075554	645	34	18	1.44 ± 0.02	12.7 ± 6.7	6.6 ± 0.5	6.2 ± 0.6	327 ± 11	1.06 ± 0.05	1360 ± 70
075555	840	21	17	1.88 ± 0.10	3.5 ± 11.0	4.7 ± 0.8	4.7 ± 0.8	146 ± 10	0.63 ± 0.05	2980 ± 300
075556	1160	33	18	4.47 ± 0.12	−0.5 ± 7.3	4.2 ± 0.5	3.2 ± 0.5	314 ± 10	0.90 ± 0.05	5000 ± 300
075557	1255	29	17	5.25 ± 0.10	17.7 ± 7.2	8.4 ± 0.6	8.1 ± 0.6	303 ± 11	1.05 ± 0.05	5000 ± 300
075558	1330	29	18	4.9 ± 0.3	8.8 ± 5.2	4.9 ± 0.4	4.9 ± 0.4	294 ± 9	0.93 ± 0.05	5300 ± 400

charge transfer shows an increase in apparent dose when higher preheat temperatures are employed (Figure 4). It is desirable to minimise thermal transfer, especially when dating contemporary sediments. For these samples, we conclude that the preheat temperature used for routine dating could be <260°C, based on the temperature interval in which D_e is independent of preheat temperature (Figure 3) and in which the apparent doses in well-bleached material are lower than 0.1 Gy (Figure 4; corresponding to an age of *c.* 100 years). Nevertheless, to minimise the chances of unexpected interference from thermal transfer, a preheat temperature of 200°C was chosen for all samples with D_e values less than ~5 Gy.

Dose recovery tests were carried out by bleaching three aliquots of each sample at room temperature, using the blue LEDs for 40 s, pausing for 10 000 s, and repeating the optical bleach for another 40 s. A known beta dose (0.5−16 Gy) was then administered and the SAR protocol used to measure the dose. A summary histogram of all the dose recovery ratios (measured/given dose) is given in Figure 5; the mean ratio is 0.98±0.01 (n=234) and *c.* 87% of the aliquots have a dose recovery ratio within the range of 0.9−1.1.

Dose rates

The annual dose rate to buried quartz grains is derived from roughly equal contributions from ^{40}K, and the ^{232}Th and ^{238}U decay series, with a small contribution from ^{87}Rb decay and cosmic rays (Aitken, 1985). The measured activity concentrations (Bq/kg) of the various radionuclide concentrations are presented in Tables 2−8, and are converted to dose rates (Gy/ka) using the conversion factors provided by Olley *et al*. (1996) and assuming that all the energy emitted by the sediment is absorbed by the sediment (the so-called infinite-matrix assumption).

The cosmic ray dose rate, which is a function of altitude, longitude, elevation and burial depth, is made up of a penetrating component that is only slowly attenuated in the surface of the Earth, and

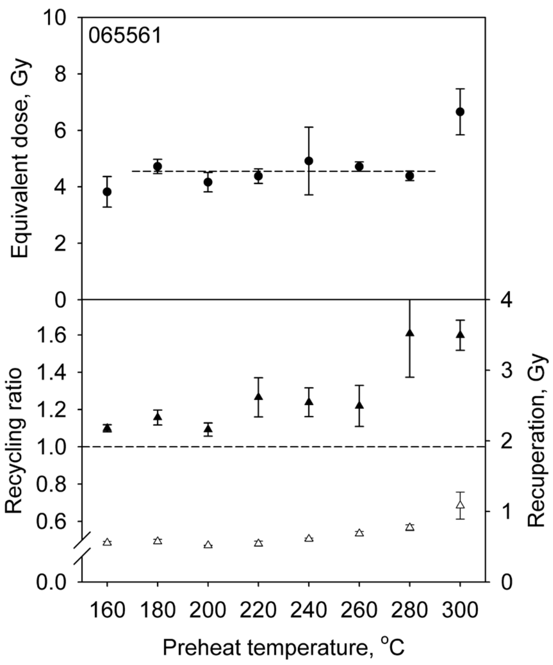

Figure 3. The variation of the equivalent dose with preheat temperature (solid circles) and the preheat plateau (dashed line). Open triangles indicate the variation of recuperation with preheat temperature and solid triangles indicate how the preheat temperature affects the recycling ratio of one of the laboratory doses

a

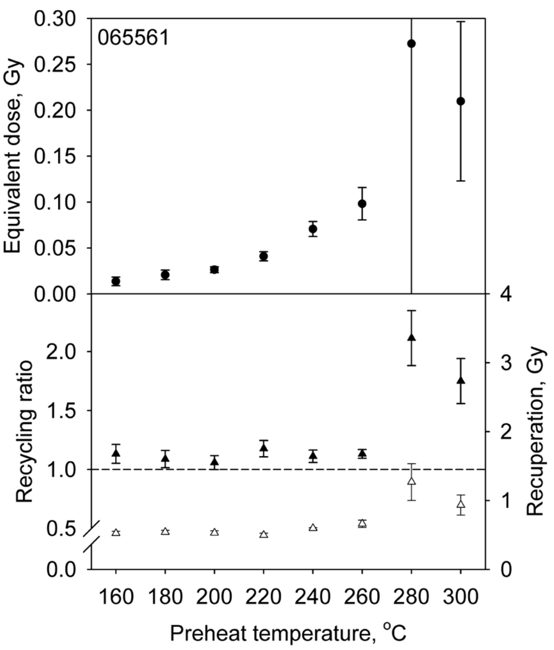

Figure 4. Dependence of the apparent D_e on preheat temperature after bleaching with blue light (the so-called thermal transfer)

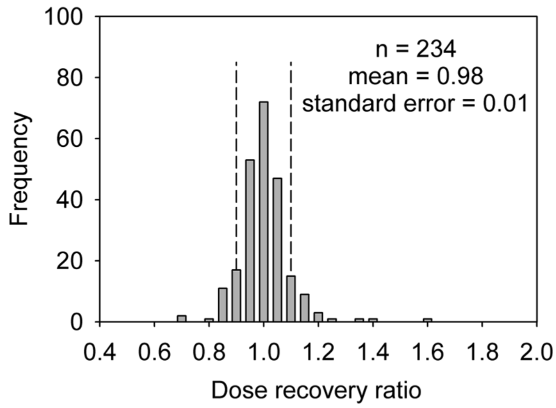

Figure 5. Summary of all dose recovery ratios. Dose recovery tests were done for all samples, typically using three aliquots per sample – 234 aliquots in total. The dashed lines mark the limit 0.9–1.1; approximately 87% of the aliquots have dose recovery ratios within these limits

soft component, which is attenuated almost entirely in the uppermost metre of sediment. Methods to calculate the cosmic ray dose rate arising from these two components are provided by Prescott and Hutton (1994). The burial depth of a sample may, however, vary considerably with time in accretionary sedimentary environments. This results in a time-dependent decrease in the contribution from the cosmic ray dose rate as the sediment progressively gets buried because of the increasing attenuation of cosmic rays with depth. However, the contribution from cosmic rays to the dose rate is small (usually <10% of the total dose rate) compared with the contributions from beta and gamma dose rate originating directly from the sediment matrix. It was therefore not considered necessary to model the temporal variation of the cosmic ray dose rate.

The presence of water in the sediment results in a dilution of the dose rate because water absorbs the energy emitted during radioactive disintegration but does not emit radiation to compensate for this absorption (Ivanovich and Harmon, 1992). All cores were taken from interdune sites with a maximum elevation of 5 m above mean sea level (Table 1). Over the period of interest, sea-level rise was largely continuous with only short periods of limited sea-level fall. For instance, during the 'Little Ice Age' it is known that sea level fell by approximately 0.5 m (Aagaard *et al*., 2007; Christiansen *et al*., 1990; Clemmensen *et al*., 1996). Present-day water-tables are all within 1 m of the interdune surfaces, even in the middle of the island. It is thus considered very unlikely that the assumed saturated water contents changed significantly with time and these values were used in dose rate calculations (cf. Aitken, 1985).

OSL chronology

The laboratory tests of the luminescence characteristics of the quartz grains show that the sediment is suitable for dating, using the SAR protocol. Dose recovery ratios (Figure 5) confirm that it is possible to measure a known laboratory dose precisely, and preheat plateaus (Figure 3) and thermal transfer plateaus (Figure 4) indicate that problems associated with unwanted charge-transfer can be avoided when preheat temperatures are chosen appropriately. The OSL ages from the seven sediment cores range between 220±20 and 15 800±1200 years (details on equivalent doses (D_e) and dose rates are presented in Tables 2–8), and these are presented as age-elevation diagrams in Figure 6. Johannessen *et al*. (2008, 2010) present a sedimentary facies model of the seven cores. Typically, the facies found in the sediment cores included: prograding/aggrading shoreface sand, transgressive/aggrading shoreface sand, fluvial channels, washover fans, swale deposits, aeolian sand and back-barrier lagoon with mudflats and sandflats. The age-elevation diagrams (Figure 6) show that there was considerable temporal and spatial variation in the rate of accretion during the Holocene.

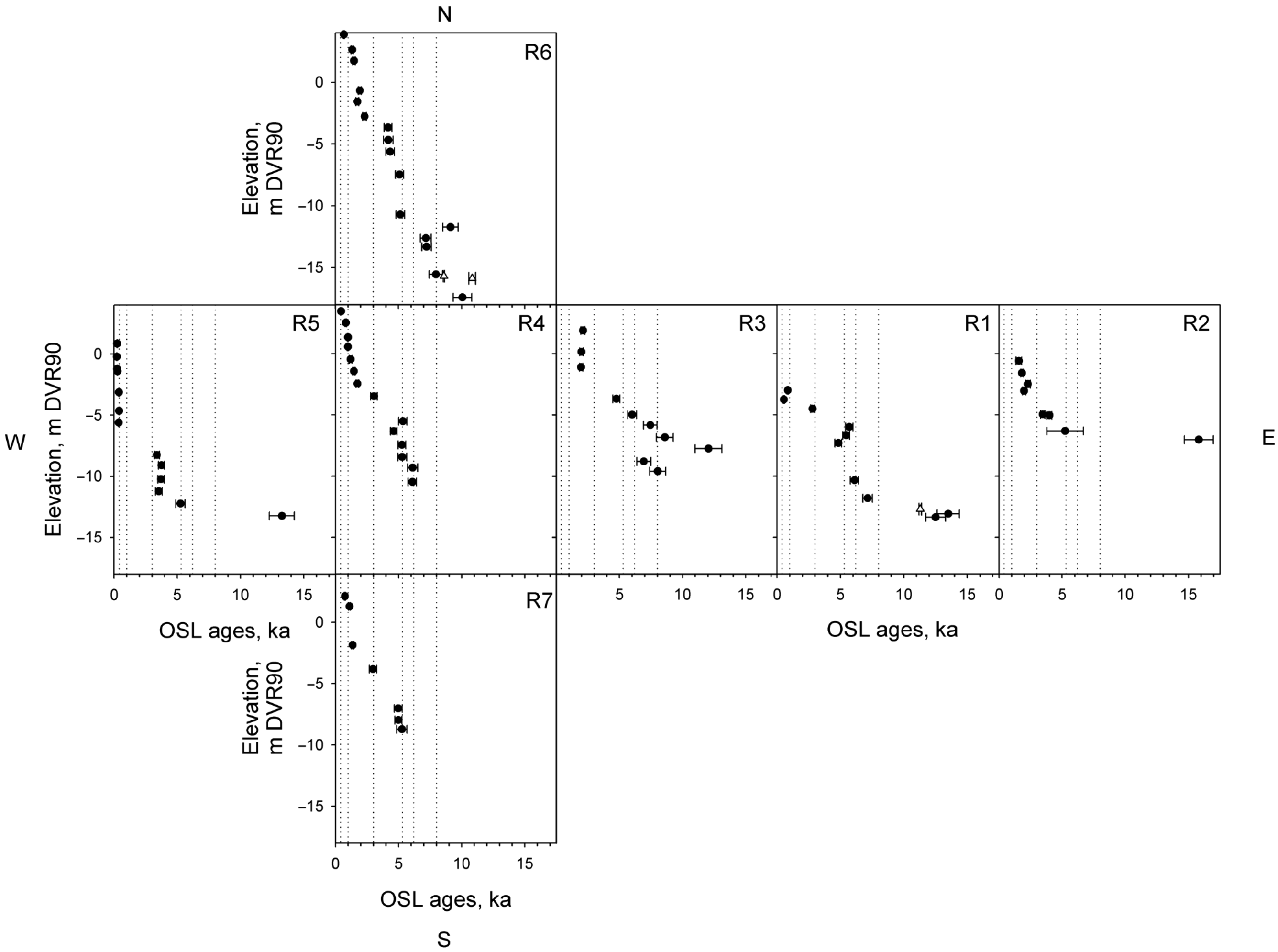

Figure 6. The variation of OSL ages with elevation (solid circles) in the top 20 m of the seven different sediment cores from Rømø and the adjacent tidal lagoon. Three independent ^{14}C ages are displayed as open triangles. The vertical dotted lines at *c.* 400, 1000, 3000, 5300, 6200 and 8000 years ago indicate six development phases

Uncertainties in the OSL ages

Uncertainties in OSL ages can be considered as a combination of experimental and systematic errors (Aitken, 1985) in both the D_e measurements and dose rate determinations. For instance, in measurements of the equivalent dose (D_e), the experimental uncertainty can be reduced by making several measurements (in practice, $n \geq 18$; see column 4 in Tables 2–8) providing a dose distribution from which the mean and standard error can be derived. However, the systematic errors in the measurement of D_e (mainly uncertainties in beta source calibration, estimated to *c.* 2%) cannot be reduced by repeated measurements. In gamma spectrometry (used to assess the dose rate) experimental uncertainties can be reduced by counting the samples for as long as possible (>24 h). However, systematic uncertainties are more difficult to assess because assumptions have to be made concerning radioactive equilibrium, changes in radioactivity with time, water content history and past changes in sedimentary density and burial depth (here sample depth and water content are assumed to have been constant with time). Experimental uncertainties (in both D_e and dose rate estimation) range between 3.5 and 12% (usually contributing *c.* 70% to the total uncertainty) and the quantifiable systematic uncertainties (e.g. water content and beta source calibration) range between 1.5 and 5% (*c.* 30% of the total uncertainty). It is also interesting to consider the contribution to the overall uncertainty from variations in some of the assumed values (burial depth and water content). If the cosmic ray dose rate contribution is set to zero (infinite burial depth) for all samples, then the OSL ages increase by only up to *c.* 10%. If the water content is varied by ±10% around the saturation value (it is considered very unlikely that this range would ever be encountered in practice) then the OSL ages are affected by ±7%. The main sources of uncertainty in the OSL ages are from measurement of D_e and estimation of water content. Uncertainties in D_e contribute, on average, *c.* 25% to the total uncertainty, whereas uncertainties in water content contribute on average *c.* 20% to the total uncertainty. The total uncertainties (quadratic sum of experimental and systematic) in our OSL ages typically range between 5 and 17% (Tables 2–8).

Independent age control

Laboratory tests of luminescence characteristics were used to assess the precision of the method, but there are no laboratory tests available with which one can test the accuracy of the ages. Results must therefore be validated by independent age control (Madsen and Murray, 2009; Murray and Olley, 2002; Wallinga, 2002). Despite the scarcity of suitable organic material, the OSL ages can be compared with three independent age estimates provided by ^{14}C dating (Table 9 and open triangles Figure 6). The

Table 9. Radiocarbon ages from Rømø-1 and Rømø-6. Note that calibrates ages (cal. BP) refers to years before AD 1950

Sample code	Sediment core	Depth (cm)	^{14}C age (yr BP)	Calibrated dates (calendar yr)	Calibrated ages (cal. BP)
KIA34848	Rømø-1	1460	9892 ± 45	9456 BC – 9255 BC	11 300 ± 100
KIA34849	Rømø-6	2085	9510 ± 80	9158 BC – 8630 BC	10 845 ± 265
KIA34850	Rømø-6	2067	7820 ± 35	6710 BC – 6588 BC	8600 ± 60

calibrated ^{14}C age of 11 300±100 years (cal. BP) in the Rømø-1 core is bracketed by OSL dates taken directly overlying and underlying the organic horizon; samples 075513 and 075514 gave OSL ages of 7100±400 years and 13500±900 years, respectively. In the Rømø-6 core there is also an agreement between OSL and ^{14}C ages; the three OSL samples taken above, between and below the two organic horizons (samples 075548, 075549 and 075550) were dated to 7200±400 years, 8000±500 years and 10 000±700 years compared with the calibrated ^{14}C ages of 8600±60 years and 10 845±265 years (cal. BP). Based on this evidence and that of Madsen *et al*. (2007) on related material, we conclude that the OSL ages are reliable.

Discussion

The OSL chronology, based on 78 absolute dates from seven sites at the barrier island Rømø and the adjacent back-barrier lagoon, shows consistent age–depth trends. The trends at Rømø-4 and Rømø-7 follow a similar pattern, even though the two cores were taken *c*. 3 km apart, giving us confidence in the results. There are few stratigraphic inversions in this study; out of 78 ages only three ages (075507, 075526, 075546) are not consistent with over/underlying ages. These may have an environmental explanation (e.g. insufficient resetting of the OSL signal during overwash events), but in all three cases there is some evidence that the problem lies in the dose rate estimation (since the D_e estimates are more consistent with the stratigraphy than the ages). Thus these inconsistencies may reflect occasional radio-analytical errors.

A considerable temporal and spatial variation in sedimentation is found at Rømø during the Holocene. For instance, at Rømø-3 wash-over deposition started *c*. 8000–6100 years ago, indicating the first appearance of a barrier island; lagoon deposition at Rømø-6 and Rømø-1 followed soon after. Between *c*. 6100 and 5300 years ago a considerable amount of sediment was deposited at Rømø-1 (lagoonal deposition) and Rømø-4 (prograding/agrading shoreface sand), but no significant deposition took place at the other five sites. In contrast, evidence of sediment deposition is seen in all sediment cores, even Rømø-5, from *c*. 5300 to 3000 years ago, resulting from considerable lateral progradation of the coast line. From *c*. 3000 to 1000 years ago, sediment deposition occurs at all sites except from Rømø-5, indicating that barrier island deposition some time around 3000 years ago may have shifted back landwards (east of Rømø-5). After *c*. 1000 years ago, sedimentation has primarily taking place as aeolian sand deposition at Rømø-4, Rømø-6 and Rømø-7 and upper shoreface sand at Rømø-5.

Periods of rapid sediment accretion are represented by a succession of similar or indistinguishable ages (Figure 6). For instance, 3 m of aeolian sand deposition occurred about 2000 years ago at Rømø-3 (sample 075519–075521), 3 m of shoreface sand was deposited about 3500 years ago at Rømø-5 (sample 065576–065579) and about 5300 years ago the sedimentation was rapid at Rømø-1 (sample 075509–075511), Rømø-4 (sample 065559–065562) and Rømø-7 (sample 075556–075558). Three metres of sediment was deposited as marine shoreface sand at Rømø-4 over a very short period, owing to a relatively rapid westward progradation of the shoreline from Rømø-3 to Rømø-4 at that time.

Preliminary geological interpretation

Over the last *c*. 8000 years, the southern North Sea coast has experienced an overall relative sea-level rise of about 17 m (Behre, 2007; Pedersen *et al*., 2009). The dynamics of relative sea-level rise together with sediment supply are amongst the most important parameters for barrier island evolution (Hoselmann and Streif, 2004) – a barrier island emerges when the sediment level exceeds the sea level. The lateral position and the spatial extension of the barrier island are related to shifts in the balances between sea level and availability of sediment, which may change the geomorphological stage from being a transgressive to a progradational barrier system or *vice versa*.

The first sign of a barrier island in this study area is at Rømø-3 *c*. 8000 years ago, where washover fans were deposited at *c*. 12 m depth in the core. Since the first appearance of Rømø, the barrier island has evolved in multiple building phases, and from its initial location at Rømø-3 the island has expanded towards west, north and south, presumably because of an abundant sediment supply. To facilitate the presentation of our data, the last *c*. 8000 years have been subdivided into six phases, based on the OSL ages of the seven sediment cores (Tables 2–8) and the facies interpretation (Johannessen *et al*., 2008, 2010). The six identified development phases are: (1) *c*. 8000–6100 years ago, (2) *c*. 6100–5300 years ago, (3) *c*. 5300–3000 years ago, (4) *c*. 3000–1000 years ago, (5) *c*. 1000–400 years ago and (6) *c*. 400–0 years ago. This subdivision is displayed as vertical dotted lines in Figure 6 and used in the following discussion. After the initial emergence of the barrier island close to Rømø-3 (prior to phase 1), lagoon deposition followed at Rømø-1 and Rømø-6 soon after, and further overwash deposition occurred at Rømø-3 in phase 1 (*c*. 8000–6100 years ago). Thus the lateral extent of the island was much smaller *c*. 8000 years ago than at present. In phase 2 (*c*. 6100–5300 years ago) the island experienced a westward progradation and marine shoreface sand started to deposit at Rømø-4 *c*. 6000 years ago; a considerable amount of sediment was deposited at Rømø-1 and Rømø-4 during phase 2, but no significant deposition took place at the other sites (see Figure 6). Rømø-3 was, however, influenced by overwash deposition throughout this phase. During the following phase 3 (*c*. 5300–3000 years ago) the island experienced further westward progradation and marine shoreface sand started to deposit at Rømø-5 *c*. 5000 years ago. During phase 3 there is evidence of pronounced sediment deposition at all the seven sites. In phase 4 (*c*. 3000–1000 years ago) the sedimentation continues at all sites except from Rømø-5, where no sediments have been preserved from this phase. This is likely due to a temporary shoreline retreat. In phase 5 (*c*. 1000−400 years ago), aeolian deposition is abundant at Rømø-4, Rømø-6 and Rømø-7 and in the last phase (*c*. 400−0 years ago) aeolian deposition primarily takes place further westward at Rømø-5.

Rømø has primarily been built on a progradational barrier system during the last *c*. 8000 years, because of an abundant sediment supply originating from the convergence of two littoral drifts just off the west coast of the island. The evolution of the barrier island has presumably resulted from a stepwise shoreface progradation caused by landward-migrating bars that have welded onto the coast. The lateral growth rate is estimated to 3 km in *c*. 1000 years (from Rømø-4 to the present coastline) and this compares well with historical map evidence and previous studies based on direct levelling (Bartholdy and Pejrup, 1994; Madsen *et al*., 2007). The abundant sediment surplus at Rømø has been able to overrule the usual transgressive effects of sea-level rise and has lead to a progradational barrier system, in which the sedimentary record is preserved.

Conclusion

The laboratory tests of luminescence characteristics have supported the reliability of the quartz OSL ages presented in this study. Preheat plateaus, thermal transfer tests and dose recovery measurements all confirmed the suitability of our measurement protocols. The stratigraphic agreement between OSL ages and ^{14}C ages gives further confidence in the OSL chronology, and it is therefore concluded that luminescence dating is well-suited for establishing precise and accurate chronologies for these barrier island deposits.

Our chronology is based on 78 OSL dates and three radiocarbon dates of the sedimentary successions of the barrier island Rømø. The OSL ages range between 220±20 and 15 800±1200 years. Rømø seems to have initially appeared *c*. 8000 years ago at a position adjacent to Rømø-3, which today coincides with the easternmost part of the island. The sediment supply was then sufficient to allow the North Sea coastline to prograde seawards (despite rising sea level) and the island has also gradually expanded towards north and south.

Most barrier islands are made up of sandy deposits; the application of OSL dating has made direct age estimations of these types of deposits possible. This technique is expected to be of great value in the reconstruction of barrier island evolution in future studies.

Acknowledgements

The study, which was a part of a larger project 'The Origin and Geneses of Coastal Barrier Systems' was financed by the Danish Natural Science Research Council (FNU) grant no. 272-05-0278. It was furthermore supported by the Nordic Centre of Excellence Programme of the Joint Committee of the Nordic Natural Science Research Councils, and Geocenter Danmark, grant no. 603-00003. The project was carried out as a joint venture between the Department of Geography and Geology (University of Copenhagen), the Geological Survey of Denmark and Greenland (GEUS) and The Nordic Laboratory for Luminescence Dating (University of Aarhus, Risø). We would therefore like to thank everyone who has been a part of this so-called OBS-group and who has participated in fruitful discussions.

References

Aagaard T, Orford J and Murray AS (2007) Environmental controls on coastal dune formation; Skallingen Spit, Denmark. *Geomorphology* 83: 29–47.

Aitken MJ (1985) *Thermoluminescence Dating*. London: Academic Press Inc., 359 pp.

Armitage SJ, Botha GA, Duller GAT, Wintle AG, Rebêlo LP and Momade FJ (2006) The formation and evolution of the barrier islands of Incaha and Bazaruto, Mozambique. *Geomorphology* 82: 295–308.

Ballarini M, Wallinga J, Murray AS, van Heteren S, Oost AP, Bos AJJ *et al.* (2003) Optical dating of young coastal dunes on a decadal time scale. *Quaternary Science Reviews* 22: 1011–1017.

Bartholdy J and Pejrup M (1994) Holocene evolution of the Danish Wadden Sea. *Senckenbergiana Maritima* 24: 187–209.

Behre KE (2007) A new Holocene sea-level curve for the southern North Sea. *Boreas* 36: 82–102.

Bird ECF (1993) *Submerging Coasts. The Effect of a Rising Sea Level on Coastal Environments*. Chichester: Wiley, 169 pp.

Bøtter-Jensen L (1997) Luminescence techniques: Instrumentation and methods. *Radiation Measurements* 27: 749–768.

Christiansen C, Dalsgaard K, Møller JT and Bowman D (1990) Coastal dunes in Denmark: Chronology in relation to sea level. *Catena* 18: 61–70.

Clemmensen LB, Andreasen F, Nielsen ST and Sten E (1996) The late Holocene coastal dunefield at Vejers, Denmark: Characteristics, sand budget and depositional dynamics. *Geomorphology* 17: 79–98.

Davis RA Jr (1994) Barrier islands systems – A geologic overview. In: Davis RA Jr (ed.) *Geology of Holocene Barrier Island Systems*. Berlin: Springer, 1–46.

Dean RG and Maurmeyer EM (1983) Models for beach profile response. In: Komar PD (ed.) *Handbook of Coastal Processes and Erosion*. Boca Raton FL: C.R.C. Press, 151–166.

Flemming BW (2002) Effects of climate and human interventions on the evolution of the Wadden Sea depositional system (southern North Sea). In: Wefer G, Berger W, Behre KE and Jansen E (eds) *Climate Development and History of the North Atlantic Realm*. Berlin: Springer, 399–413.

Gehrels WR, Szkornik K, Bartholdy J, Kirby JR, Bradley SL, Marshall WA *et al.* (2006) Late Holocene sea-level changes and isostasy in western Denmark. *Quaternary Research* 66: 288–302.

Hoselmann C and Streif H (2004) Holocene sea-level rise and its effects of the mass balance of coastal deposits. *Quaternary International* 112: 89−103.

Intergovernmental Panel on Climate Change (IPCC) (2007) Climate change 2007. In: Solomon S, Qin D, Manning M, Chen Z, Marquis M, Averyt KB *et al.* (eds). *The Physical Science Basis. Contribution of Working Group I to the Fourth Assessment Report of Intergovernmental Panel on Climate Change*. Cambridge and New York: Cambridge University Press.

Ivanovich M and Harmon RS (1992) *Uranium-series Disequilibrium*. Oxford: Clarendon Press, 910 pp.

Johannessen PN, Nielsen LH, Nielsen L, Møller I, Pejrup M, Andersen TJ *et al.* (2008) Sedimentary facies and architecture of the Holocene to recent Rømø barrier island in the Danish Wadden Sea. *Geological Survey of Denmark and Greenland Bulletin* 15: 49–52.

Johannessen PN, Nielsen LH, Nielsen L, Møller I, Pejrup M and Andersen TJ (2010) Architecture of an Upper Jurassic barrier island sandstone reservoir, Danish Central Graben: Implications of a Holocene–recent analogue from the Wadden Sea. In: Vining BA (ed.) *Petroleum Geology: From Mature Basins to New Frontiers*. Proceedings of the 7th Petroleum Geology Conference. London: Geological Society, in press.

Komar PD, Lanfredi N, Baba M, Dean RG, Dyer K, Healy T *et al.* (1991) The response of beaches to sea-level changes: A review of predictive models. *Journal of Coastal Research* 7: 895–921.

Leatherman SP (1983) Barrier-island evolution in response to sea-level rise – A discussion. *Journal of Sedimentary Petrology* 53: 1026–1031.

Lopez GI and Rink WJ (2008) New quartz optical stimulated luminescence ages for beach ridges on the St. Vincent Island Holocene strandplain, Florida, United States. *Journal of Coastal Research* 24: 49–62.

Madsen AT and Murray AS (2009) Optically stimulated luminescence dating of young sediments: A review. *Geomorphology* 119: 3–16.

Madsen AT, Murray AS and Andersen TJ (2007) Optical dating of dune ridges on Rømø, a barrier island in the Wadden Sea, Denmark. *Journal of Coastal Research* 23: 1259–1269.

Moritz E (1903) *Die Nordseeinsel Röm*. Mitteilungen der Geographischen Gesellschaft in Hamburg 19, 210 pp. (in German).

Murray AS and Olley JM (2002) Precision and accuracy in the optically stimulated luminescence dating of sedimentary quartz: A status review. *Geochronometria* 21: 1–16.

Murray AS and Wintle AG (2000) Luminescence dating of quartz using an improved single-aliquot regenerative-dose protocol. *Radiation Measurements* 32: 57–73.

Murray AS and Wintle AG (2003) The single aliquot regenerative dose protocol: Potential for improvements in reliability. *Radiation Measurements* 37: 377–381.

Murray AS, Marten R, Johnston A and Martin P (1987) Analysis for naturally occuring radionuclides at environmental concentrations by gammaspectrometry. *Journal of Radioanalytical and Nuclear Chemistry* 115: 263–288.

Nielsen L, Møller I, Nielsen LH, Johannessen PN, Pejrup M, Andersen TJ *et al.* (2009) Integrated ground-penetrating radar and sedimentological studies of a Wadden Sea barrier island. *Journal of Applied Geophysics* 68: 47–69.

Nummedal D (1983) Barrier islands. In: Komar PD (ed.) *Handbook of Coastal Processes and Erosion*. Boca Raton FL: C.R.C. Press, 77–121.

Oertel GF (1985) The barrier island system. *Marine Geology* 63: 1–18.

Olley JM, Murray AS and Roberts RG (1996) The effects of disequilibrium in the uranium and thorium decay chains on burial dose rates in fluvial sediments. *Quaternary Science Reviews* 15: 751–760.

Pedersen JBT, Svinth S and Bartholdy J (2009) Holocene evolution of a drowned melt-water valley in the Danish Wadden Sea. *Quaternary Research* 72: 68−79.

Prescott JR and Hutton JT (1994) Cosmic-ray contributions to dose rates for luminescence and ESR dating – Large depths and long-term time variations. *Radiation Measurements* 23: 497−500.

Reimer PJ, Baillie MGL, Bard E, Bayliss A, Beck JW, Bertrand CJH *et al.* (2004) INTCAL04 terrestrial radiocarbon age calibration, 0–26 cal kyr BP. *Radiocarbon* 46(3): 1029−1058.

Rhodes EJ (2000) Observations of thermal transfer OSL signals in glacigenic quartz. *Radiation Measurements* 32: 595–602.

Thom BG (1983) Transgressive and regressive stratigraphies of coastal sand barriers in southeast Australia. *Marine Geology* 56: 137–158.

Wallinga J (2002) Optically stimulated luminescence dating of fluvial deposits: A review. *Boreas* 31: 303–322.

Wallinga J, Murray AS and Duller GAT (2000) Underestimation of equivalent dose in single-aliquot optical dating of feldspars caused by preheating. *Radiation measurements* 32: 691–695.

Wintle AG (1997) Luminescence dating: Laboratory procedures and protocols. Radiation Measurements 27: 769–817.